Environmental Science & Technology

pubs.acs.org/est

Article

New Insights into Thermal Degradation Products of Long-Chain Per- and Polyfluoroalkyl Substances (PFAS) and Their Mineralization Enhancement Using Additives

Runze Sun, Ali Alinezhad, Mohammednoor Altarawneh, Mohamed Ateia, Jens Blotevogel, Jiamin Mai, Ravi Naidu, Joseph Pignatello, Anthony Rappe, Xuejia Zhang, and Feng Xiao*

Cite This: https://doi.org/10.1021/acs.est.4c05782

Read Online

ACCESS | Metrics & More | Article Recommendations | Supporting Information

ABSTRACT: The products of incomplete destruction (PIDs) of per- and polyfluoroalkyl substances (PFAS) represent a substantial ambiguity when employing thermal treatments to remediate PFAS-contaminated materials. In this study, we present new information on PIDs produced in both inert and oxidative environments from five long-chain PFAS, including three now regulated under the U.S. Safe Drinking Water Act, one cationic precursor compound, and one C10 PFAS. The data did not support the generation of tetrafluoromethane from any of the studied PFAS, and carbonyl fluoride was found only from potassium perfluorooctanesulfonate (K-PFOS) when heated in air in a narrow temperature range. Oxidative conditions (air) were observed to facilitate PFAS thermal degradation and accelerate the mineralization of K-PFOS. Spectroscopic data suggest that PFAS thermal degradation is initiated by the cleavage of bonds that form perfluoroalkyl radicals, leading to organofluorine PIDs (e.g., perfluoroalkenes). In air, perfluoroalkyl radicals react with oxygen to form oxygen-containing PIDs. The mineralization of PFAS was enhanced by adding solid additives, which were categorized as highly effective (e.g., granular activated carbon (GAC) and certain noble metals), moderately effective, and noneffective. Remarkably, simply by adding GAC, we achieved >90% mineralization of perfluorooctanoic acid at 300 °C and ~1.9 atm within just 60 min without using water or solvents.

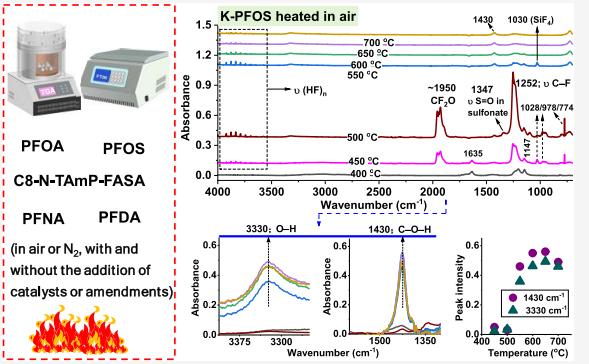

KEYWORDS: *PFOA, PFSA, yield, unsaturated products, PFNA, PFDA, N-TAmP-FASA*

INTRODUCTION

Per- and polyfluoroalkyl substances (PFAS), known for their strong carbon−fluorine bonds and surfactant capabilities, are widely used in various industrial and consumer products, such as food packaging, nonstick cookware, carpets, cosmetics, and aqueous film-forming foams (AFFFs).[1−3] In recent years, PFAS have raised significant environmental and health concerns due to their high stability, potential for bioaccumulation, and widespread detection in natural waters,[4−6] precipitation,[7−10] wastewater,[11−13] soil,[14−16] biosolids,[17,18] municipal solid wastes,[19] plants,[20,21] and animals.[22−26] In April 2024, the U.S. Environmental Protection Agency (USEPA) finalized the regulation of six PFAS, including perfluorooctanoic acid (PFOA), perfluorooctanesulfonic acid (PFOS), and perfluorononanoic acid (PFNA), under the Safe Drinking Water Act.[27] PFOA and PFOS have also been designated as hazardous substances under the Comprehensive Environmental Response, Compensation, and Liability Act,[28] highlighting ongoing regulatory responses to these concerns. Nevertheless, the widespread distribution and resilience of PFAS present significant challenges in terms of management and control, underscoring the pressing need to develop and assess effective remediation technologies.[29−37]

As of now, the USEPA considers granular activated carbon (GAC), ion exchange (IX), and high-pressure membrane filtration the best available techniques for removing PFAS from natural waters.[38] However, once spent, materials like GAC and IX beads require careful handling to ensure safe disposal and prevent secondary contamination. These materials concentrate PFAS, which could be released back into the environment if not properly managed. To tackle this issue, various thermal-based cleanup methods targeting PFAS-contaminated spent media have been investigated and demonstrated potential in recent laboratory and field tests.[39−46]

Received: June 9, 2024
Revised: November 18, 2024
Accepted: November 25, 2024

The application of thermal treatments extends beyond the spent media. Thermal technologies—incineration,[47−50] pyrolysis,[51−54] smoldering,[55,56] dry air oxidation,[42,43,57] sonolysis,[58−60] ball milling,[61−63] thermal desorption,[64−66] plasma,[67−69] hydrothermal treatment at elevated pressure (e.g., 16 MPa),[45,70−73] and supercritical water oxidation[72,74−77]—have been evaluated for their effectiveness on diverse vectors of PFAS, including soil, biosolids, and municipal solid wastes. The apparent half-life of PFOA heated in air at 400 °C is 3.7 ± 0.37 min,[51] while for the potassium salt of PFOS (K-PFOS) at 500 °C, it is 3.1 ± 0.58 min,[51] demonstrating the efficacy of thermal treatment in decontaminating PFAS-contaminated solid materials even at moderate temperatures.

While effective, thermal treatments are not free from challenges. The formation of volatile products of incomplete destruction (PIDs) from PFAS is particularly concerning because they include greenhouse gases such as perfluorocarbons (PFCs) and hydrofluorocarbons (HFCs). In one study utilizing real-time Fourier-transform infrared (FTIR) spectroscopy, tetrafluoromethane (CF_4), the longest-lived greenhouse gas, and carbonyl fluoride (CF_2O), a highly toxic compound,[78] were identified during the pyrolysis and combustion of short-chain perfluoroalkyl carboxylic acids (PFCAs).[79] Weber and colleagues conducted a series of experiments via thermogravimetric analysis coupled with FTIR (TGA-FTIR) for the simultaneous and continuous real-time analysis of the volatile PIDs of PFOA and PFOS (the acid form).[64,80−82] Their findings consistently demonstrated the formation of perfluoroheptanoyl fluoride ($C_7F_{14}O$) from PFOA, perfluorooctanoyl fluoride ($C_8F_{16}O$) from PFOS, and CF_2O from both compounds during thermal processes. Additionally, CF_4 was identified from PFOA when heated under oxidative conditions.[80]

Meanwhile, in a separate approach, Hughey et al. employed sampling bags to capture gaseous PIDs of K-PFOS, which were subsequently analyzed by FTIR.[83] Their research identified several perfluoroalkenes, including C_2F_4, perfluorooct-2-ene, hexafluoropropene, and perfluorooct-1-ene, as the thermal decomposition products of PFOS. Notably, neither CF_4 nor CF_2O were detected in their study.[83]

Other investigations, employing non-FTIR methods such as gas chromatography and high-resolution mass spectrometry (GC−HRMS),[84] pyrolysis−GC−MS,[85] and gas-phase nuclear magnetic resonance spectroscopy (NMR),[86] did not detect CF_4 and CF_2O under pyrolysis[85,86] or oxidative[84] heating conditions during the treatment of PFOA or PFAS mixture.

It is likely that some (short-lived) PIDs may be detectable by real-time FTIR technologies (e.g., TGA-FTIR), not by other techniques. This variability in data highlights a crucial gap in our understanding of the PIDs of PFAS. To address this knowledge gap, this study utilized TGA−FTIR to investigate the PIDs of PFAS generated under both pyrolytic and combustion conditions. TGA−FTIR allows for the analysis of PFAS weight loss upon heating and real-time monitoring of gases evolved, as detected by FTIR. To our knowledge, this study is the first to present spectroscopic information on the PIDs of PFNA, perfluorodecanoic acid (PFDA), and an AFFF-relevant cationic PFAS.

The second objective of this study was to explore strategies for enhancing the thermal degradation of PFAS using solid catalysts and additives, which may lower the temperature required for mineralization and potentially steer degradation away from undesirable pathways. A recent study has demonstrated that hydrothermal decomposition of PFOA at reduced temperatures is markedly accelerated in the presence of dimethyl sulfoxide, a polar aprotic solvent.[87] However, the use of organic solvents like dimethyl sulfoxide often raises concerns regarding environmental impact and recovery challenges. From an engineering perspective, solid catalysts may be preferred for the thermal treatment of PFAS-containing materials.

The potential of cost-effective solid catalysts has not been fully realized, presenting an opportunity for major advancements in this field. Prior research has explored three types of catalysts or additives—pure platinum (Pt),[79] alumina (Al_2O_3),[88] and alkali and alkaline-earth metal additives[73,88−91]—demonstrating that suitable additives can improve the thermal degradation of PFAS while reducing the production of PIDs. This study contributes to the existing literature by evaluating, for the first time, the effects of various conventional solid catalysts and additives used in chemical and thermal processes (e.g., cracking and hydrogenation),[92−103] including palladium (Pd) on Al_2O_3 (Pd/Al_2O_3), Pt/Al_2O_3, silica−alumina catalyst support, and zeolite Y. We also included biochar to simulate the black carbon in natural soils, which is typically produced from organic matter through pyrolysis under limited oxygen conditions. Natural chars are commonly found in soils,[104] originating from past wildfires, land clearing, and the burning of crop residues.[105−110] Char black carbon contributes to 30−50% of the soil organic carbon in specific regions, like the soils of the Midwest prairies.[111,112] The polyaromatic surface of biochar is believed to facilitate the redox transformation of organic compounds by acting as an electron shuttle, thereby accelerating the process.[113−115] Lastly, we included three commonly used GAC samples, including HD4000, Filtrasorb 200 (or F200), and Norit 400 made by leading manufacturers.

We focused on three essential criteria in identifying appropriate additives for enhancing PFAS thermal mineralization: the ability to promote PFAS mineralization at low to moderate temperatures with a low environmental footprint, effectiveness across different PFAS classes, and cost efficiency. This exploration was motivated by the need to identify methods that not only effectively degrade PFAS but also do so in an environmentally friendly manner, thereby addressing one of the crucial aspects of PFAS management: the minimization of PIDs.

MATERIALS AND METHODS

PFAS. The test chemical set (Table S1 of the Supporting Information, SI) included PFCAs in the acid form (PFOA, PFNA, PFDA, and perfluoroundecanoic acid (PFUnDA)), K-PFOS, and *N*-(3-perfluoroalkylsulfonamidopropan-1-yl)-*N*,*N*,Ntrimethylammonium (C8-*N*-TAmP-FASA[116]). C8-*N*-TAmP-FASA is also named as perfluorooctanesulfonamido ammonium salt in other studies.[57,117] The melting points of these compounds vary significantly: PFOA melts between 48.4 and 51.6 °C, PFNA between 76.8 and 78.8 °C, PFDA between 89.2 and 89.6 °C, PFUnDA between 108.8 and 109.8 °C, C8-*N*-TAmP-FASA between 144.1 and 146.3 °C, and K-PFOS between 282.6 and 282.7 °C.[39] The melted compounds begin to vaporize at temperatures close to their boiling points and degrade mainly in the gas phase,[39] with PFCAs starting to degrade between 150 and 200 °C, C8-N-TAmP-FASA at ∼250 °C, and K-PFOS at ∼400 °C.[39] PFUnDA was only included in the catalyst/additive experiments.

https://doi.org/10.1021/acs.est.4c05782
Environ. Sci. Technol. XXXX, XXX, XXX−XXX

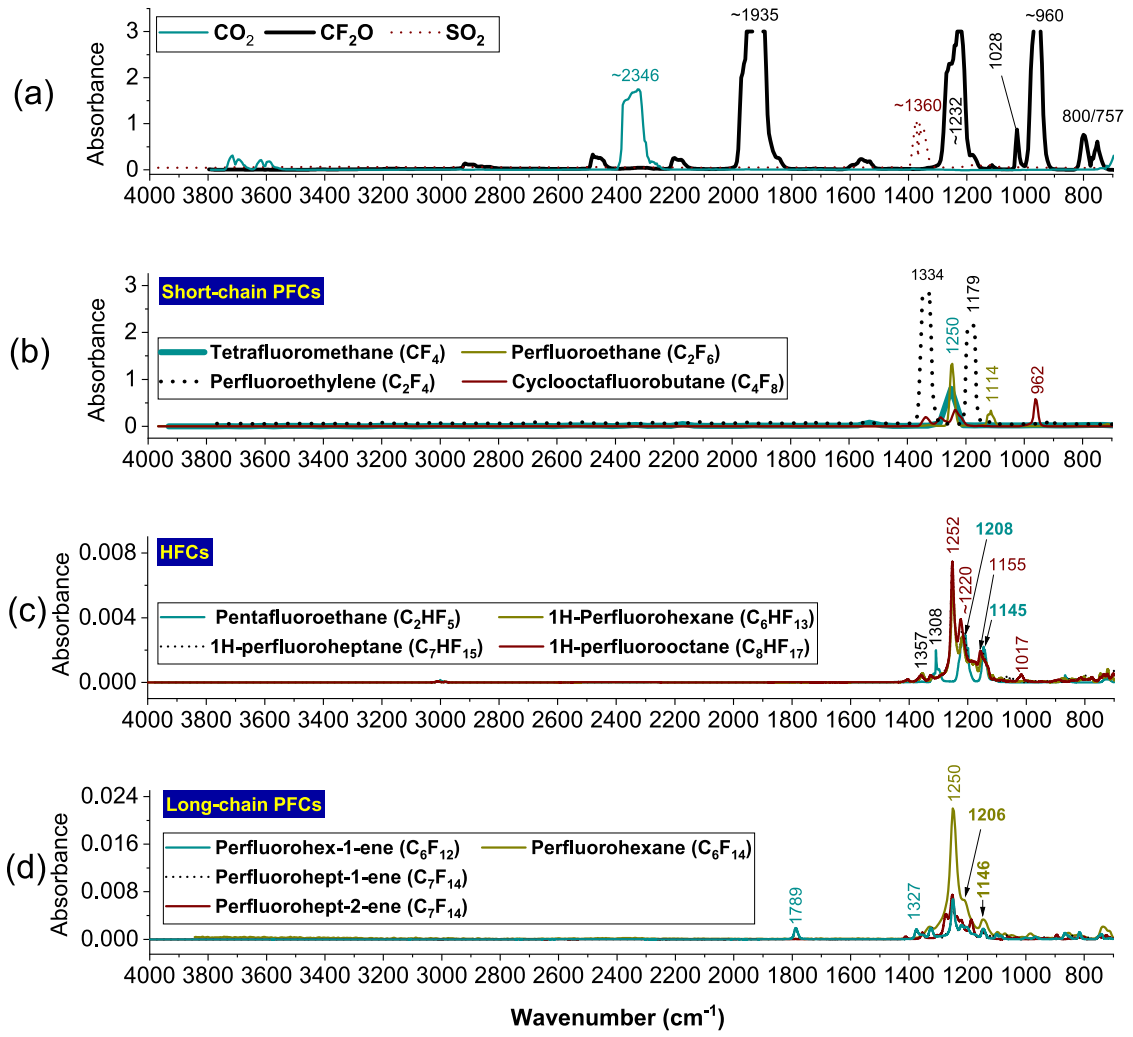

Figure 1. Panels (a–d) display the reference FTIR spectra[118,120−125] for various possible species generated from PFAS during thermal treatments, including short-chain PFCs, HFCs, and long-chain PFCs.

Catalysts and Additives. A variety of commercial catalysts and additives were examined, including molecular sieve rods, hydrogen zeolite Y, Pd/Al_2O_3, Pt/Al_2O_3, and silica–alumina catalyst support. Additional materials, such as biochar made from pecan shells, various GAC samples, iron filings, and a specific polymer (XAD-2 resins), were also tested. Characteristics of these catalysts and additives can be found in the SI.

Thermal Treatment Conditions. Two groups of thermal treatments of PFAS were conducted. In the first experimental setup, PFAS samples—with or without catalysts/additives—were dried, ground finely to increase surface area, and then subjected to thermal analysis using a TGA device (Q600 SDT TA Instruments) from room temperature to 700 °C at a rate of 10 °C/min in either a N_2 or air atmosphere. Using a temperature ramp during TGA analysis prevents rapid degradation and allows a more detailed analysis of evolved gases, providing clear insights into PID composition throughout decomposition stages.

The gases that evolved during heating were analyzed in real-time using a FTIR spectrometer (PerkinElmer Spectrum ONE FTIR) at a resolution of 2 cm^{-1}, interfaced with the TGA. Quality control measures included using a PFAS-free blank control sample (Figure S1), comparing our FTIR spectra with reference spectra (Figures S2 and S3), and cross-checking—for instance, if a peak appears in a specific group of PFAS but not in others, it is likely associated with that group of PFAS or their PIDs. A complete methodology on sample preparation and TGA–FTIR settings can be found in the SI. Figures S4–S22 illustrate the weight loss of PFAS during thermal treatments.

Recognizing the semiquantitative nature of FTIR technologies, we also carried out a second group of experiments to confirm the TGA-FTIR observations regarding the impact of catalysts/additives on PFAS mineralization. The second set of experiments adhered to a previously established protocol.[44,57] Briefly, a known quantity of PFOA alone or mixed with a catalyst/additive was placed in a sealed 300 mL vessel and heated in a muffle furnace (Neytech, Vulcan 3–550, USA) from room temperature to a preset temperature at a 10 °C/min. The yield of inorganic fluorine (F) released from PFOA degradation was measured to assess the effectiveness of the process.

Measurement of F. Samples from the second set of experiments were processed and analyzed using a Mettler Toledo pH/mV Meter equipped with a *F* ion-selective electrode, as detailed in our previous studies[39,51] and the SI. The total apparent yield (%) of *F* (mol) from a PFAS with (2*n*

https://doi.org/10.1021/acs.est.4c05782
Environ. Sci. Technol. XXXX, XXX, XXX−XXX

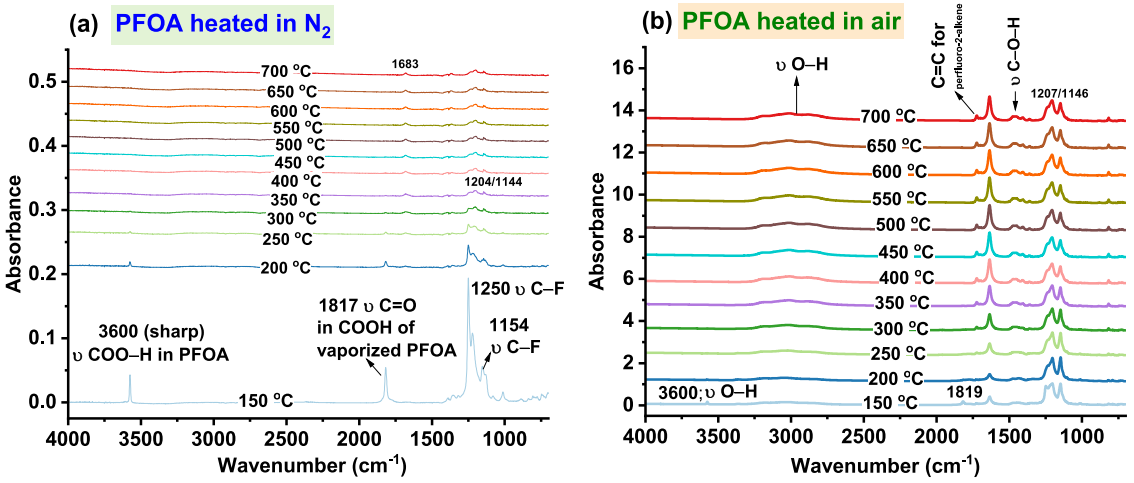

Figure 2. TGA−FTIR spectra of PFOA when heated at various temperatures ranging from 150 to 700 °C in N_2 (panel a) and air (panel b) environments.

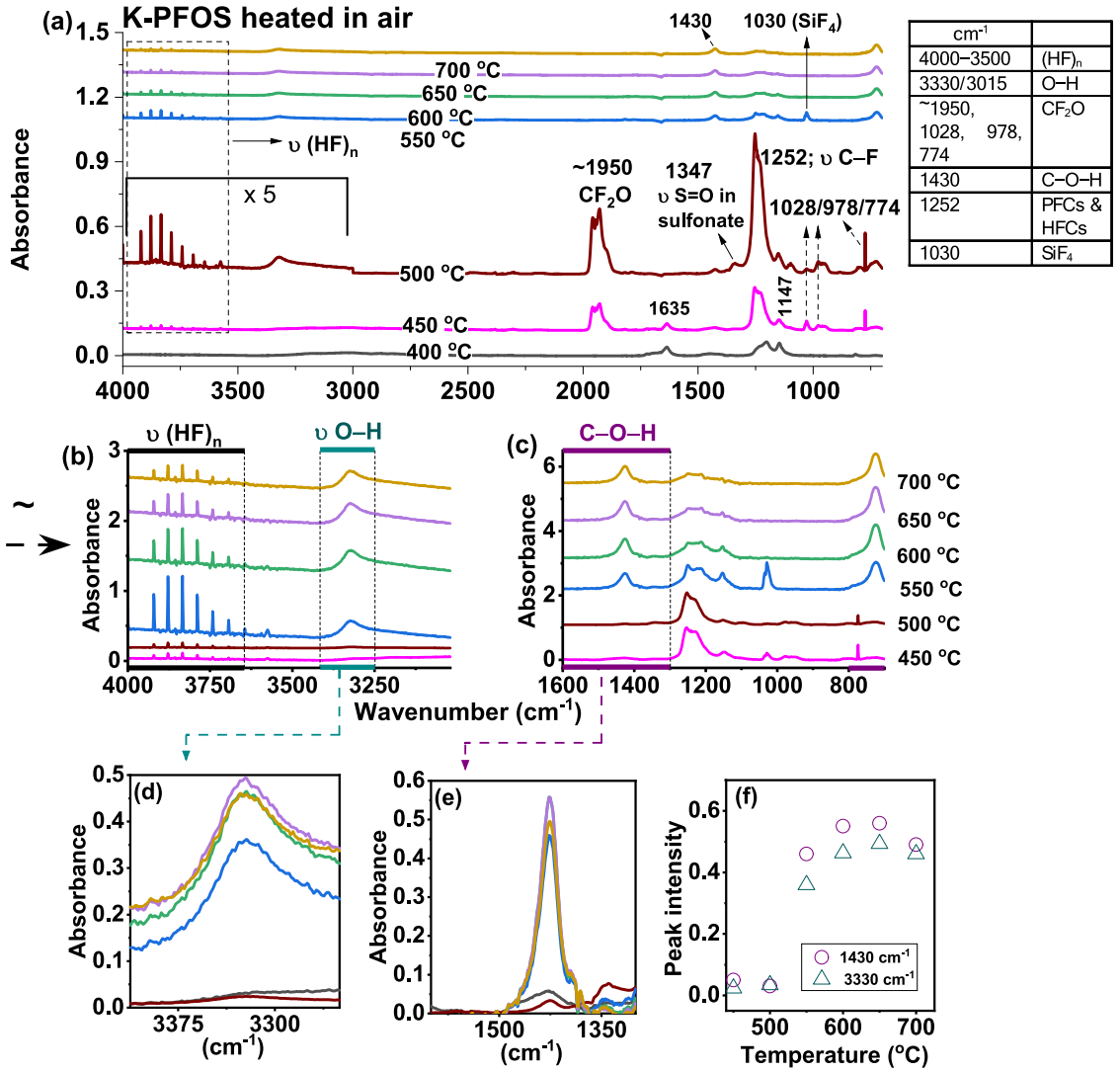

Figure 3. (a): TGA−FTIR spectra of K-PFOS when heated at various temperatures ranging from 400 to 700 °C in air. To highlight the HF formation, we have amplified the peak absorbance values between 4000 and 3000 cm^{-1} 5-fold for the spectrum at 500 °C. Panels (b) and (c): normalized FTIR in the wavenumber range of 4000−3000 and 1600−1300 cm^{-1}. Panels (d−f): the peak intensities as a function of the treatment temperature. Figure S23 shows TGA−FTIR spectra of K-PFOS heated in N_2. Table S2 presents the assignments of FTIR peaks for all PFAS analyzed in this study.

https://doi.org/10.1021/acs.est.4c05782
Environ. Sci. Technol. XXXX, XXX, XXX−XXX

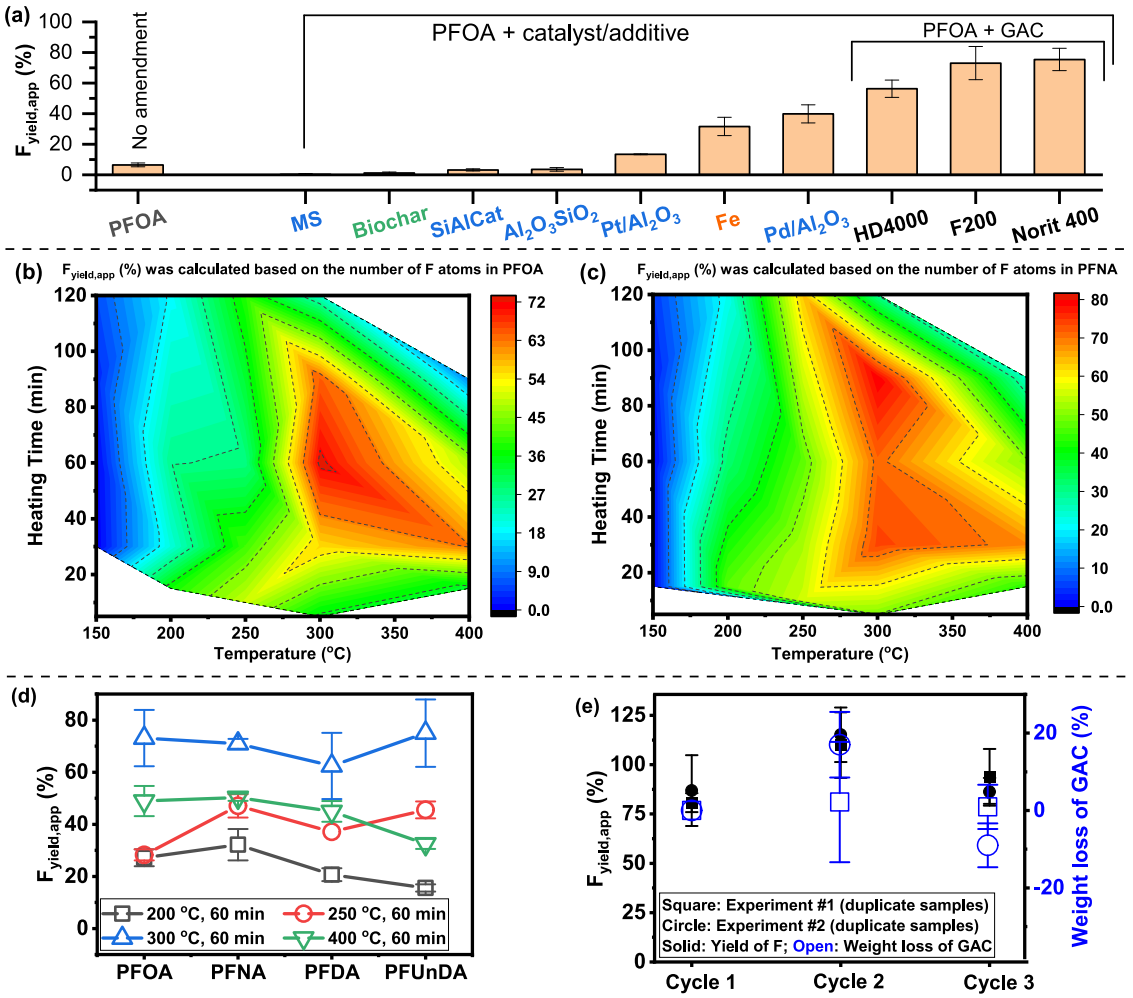

Figure 4. (a): Screening of commercial catalysts (in blue) and other additives in altering the mineralization or defluorination of PFOA heated at 300 °C for 60 min in air. Commercial catalysts: MS, molecular sieve; SiAlCat, silica−alumina catalyst support; $Al_2O_3SiO_2$, hydrogen zeolite Y; Pt/Al_2O_3, Pt on alumina; Pd/Al_2O_3, Pd on alumina. Other additives: BC, biochar; Fe, iron filings; and three mainstream GAC samples. (b, c): Contour maps showing the percentage apparent yield of F ($F_{yield,app}$) during the thermal treatment of PFOA and PFNA, respectively, across a range of temperatures and heating durations with the presence of GAC. (d): Comparative $F_{yield,app}$ from various perfluorinated compounds (PFOA, PFNA, PFDA, and PFUnDA) at four different temperatures over a 60 min heating period, with the presence of GAC (F200). (e): Cyclic stability of GAC in the catalytic degradation of PFOA at 300 °C for 60 min; solid symbols represent $F_{yield,app}$, and open symbols indicate the weight loss of GAC during repeated uses.

+ 1) F atoms was calculated from the initial mass (M_{PFAS}, mol) of PFAS

$$F_{yield,app}(\%) = \frac{M_F}{(2n+1) \times M_{PFAS}} \times 100\% \quad (1)$$

RESULTS AND DISCUSSION

Reference FTIR Spectra of PFCs, HFCs, and Other Potential Thermal Degradation Products of PFAS. We begin with a brief overview of the FTIR spectra of reference compounds gathered from the U.S. National Institute of Standards and Technology database[83,118−125] and a recent study by the U.S. Pacific Northwest National Laboratory.[120] The spectrum[79,118] of CF_2O exhibits a prominent absorption near 1935 cm^{-1}, characteristic of the C═O stretching vibration, with additional peaks at ∼1232 and ∼1028 cm^{-1} representing the stretching and bending vibrations of C−F (Figure 1a). The spectrum of SiF_4 shows a sharp and intense peak at ∼1030 cm^{-1},[119,126] attributable to the stretching vibration of the strong Si−F bond (Figure 1a).

Characteristic peaks at ∼1250 and 1114 cm^{-1} were observed in both PFCs (Figure 1b,d)[120,122−125] and HFCs (Figure 1c).[120,121] Compared to short-chain PFCs, long-chain PFCs and HFCs exhibit two characteristic peaks at 1220−1206 and 1155−1145 cm^{-1} (Figure 1c). The spectrum of CF_4 is noted for a single peak at 1250 cm^{-1}.

For perfluoroalkenes, the peaks at 1789 and 1720 cm^{-1} represent the C═C stretch of a double bond in perfluoro-1-alkenes (e.g., perfluorohept-1-ene) and perfluorohept-2-ene, respectively. Cyclooctafluorobutane (C_4F_8) displays a dominant peak at 962 cm^{-1} (Figure 1b).

Thermal Degradation Products of PFOA Investigated by TGA-FTIR. Detailed investigations focused on the thermal decomposition of PFOA and K-PFOS across a range of temperatures. Panels (a) and (b) in Figure 2 present the FTIR spectra of PFOA when heated up to 700 °C in N_2 and air, respectively. In N_2, the spectrum for PFOA at 150 °C is very similar to the reference spectrum,[127] suggesting little to no decomposition at this temperature. The results align with our previous observation[43] that the thermal degradation of PFOA

https://doi.org/10.1021/acs.est.4c05782
Environ. Sci. Technol. XXXX, XXX, XXX−XXX

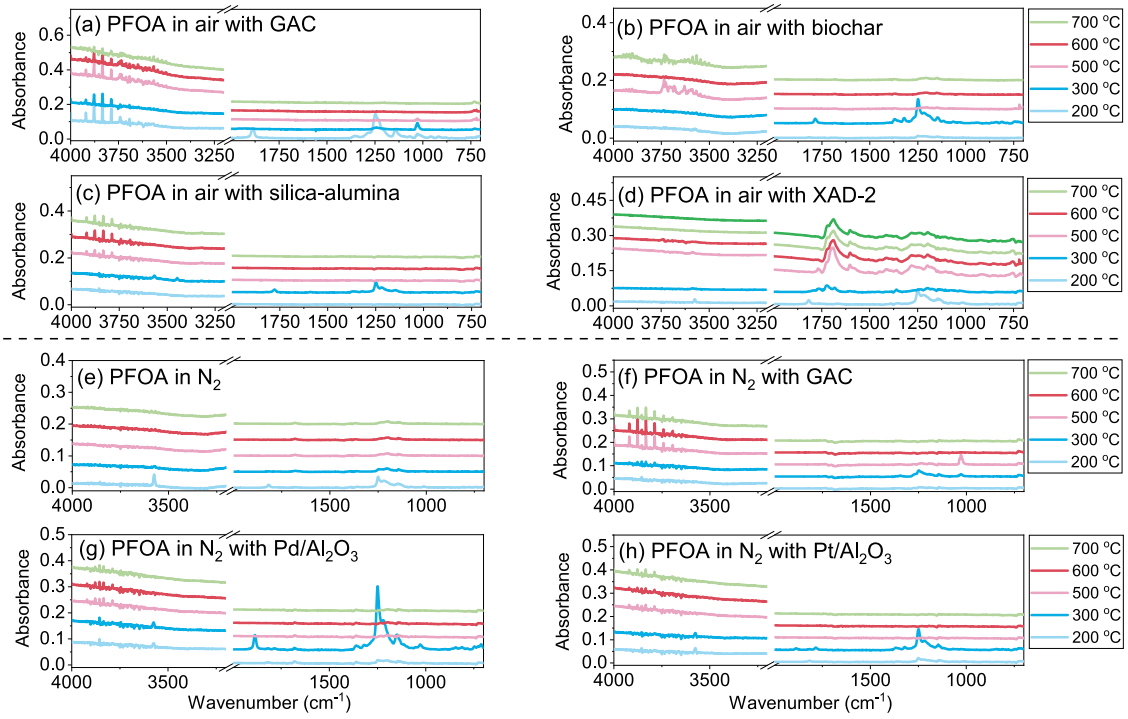

Figure 5. FTIR spectra showcasing the thermal degradation of PFOA and its PIDs formed at various temperatures in different atmospheres and in the presence of an additive.

is either thermodynamically or kinetically unfavorable at 150 °C. Above 150 °C, characteristic peaks of PFOA associated with the O−H stretch at 3600 cm^{-1}, the C═O stretch at 1817 cm^{-1}, and CF_3 vibrations around 1250 cm^{-1} began to decline in intensity, pointing to initiation of thermal degradation (Figure 2a).

Simultaneously, new peaks emerged at ∼1205 and ∼1145 cm^{-1} (Figures 1c and 2). Weber et al. recently identified perfluorooctanoyl fluoride ($C_8F_{16}O$) from PFOS in thermal processes, based on peaks observed at approximately 1207 and 1145 cm^{-1} (both C−F stretching) and at ∼1879 cm^{-1} (stretching vibration of the ketone C═O bond).[64,81] The absorbance at ∼1879 cm^{-1} falls slightly outside the typical range for ketone C═O bonds (1775−1650 cm^{-1}).[128]

In comparison, the thermal degradation of PFOA in the presence of air began at 150 °C, as evidenced by the diminishing peak (∼1819 cm^{-1}) associated with the C═O bond in PFOA's carboxyl group (Figure 2b). The emergence of new peak(s) at ∼1723 cm^{-1} (νC═C) could signify the formation of perfluoro-2-alkene, such as perfluorohept-2-ene (C_7F_{14}) (Figure S24). FTIR peaks of HF and CO_2 were not observed when PFOA was heated alone in N_2 or air (Figure 2). As shown below, the yield of F from PFOA heated alone is quite low. Carboxyl radicals, if released from PFOA via the decarboxylation pathway, may recombine with some nonpolar degradation products to form short-chain homologues; we previously demonstrated the formation of short-chain homologues from PFOA upon heating.[42,43] This might explain the absence of CO_2 peaks in Figure 2. Collectively, these findings demonstrate that the degradation of vaporized PFOA begins at approximately 150 °C, accompanied by an increasing presence of PIDs.

Thermal Degradation Products of K-PFOS Investigated by TGA-FTIR. Figures S23 and 3 present the FTIR spectra of K-PFOS when heated up to 700 °C in N_2 and air, respectively. In a N_2 atmosphere, the stability of K-PFOS was evident up to approximately 400 °C, as peaks for the S═O stretch in sulfonate at 1347 cm^{-1} and the C−F stretch at 1154 and 1250 cm^{-1} for CF_2 and CF_3 groups, respectively, maintained their presence (Figure S23). As the temperature increased above 500 °C, the characteristic peaks of K-PFOS began to fade and peaks (1500 and 1000 cm^{-1}) corresponding to potential PIDs began to emerge.

The decomposition pattern of K-PFOS in air differs significantly from that in N_2, with some new peaks being only detected under the oxidative condition. The peaks at ∼1950, 1028, 978, and 774 cm^{-1} represent CF_2O, which was observed only when K-PFOS was heated at 450 and 500 °C in air. It was not detected in PFCAs (Figures 4, 5, S25, and S26), C8-N-TAmP-FASA (see below), or when K-PFOS was heated in N_2 (Figure S23) or in air at >500 °C (Figure 3). These findings suggest that CF_2O formation is species-dependent, temperature-dependent and sensitive to the presence of oxygen.

Furthermore, the medium peak at 1430 cm^{-1} (C−O−H bending)[128] confirms the emergence of oxygen-containing PIDs in an oxidative environment, akin to the observations with PFOA. Additionally, peaks between 4000 and 3500 cm^{-1} corresponding to HF or $(HF)_n$ are particularly noteworthy. HF is known to self-associate in the vapor phase, forming $(HF)_n$ through strong hydrogen bonds.[129,130] These clusters can show a range of interactions, leading to multiple peaks in the FTIR spectrum in that region.[129,130] The appearance of $(HF)_n$ highlights the influence of oxygen in promoting the decomposition and mineralization of K-PFOS.

To enhance the visibility of subtle changes observed in the spectra (Figure 3a), we normalized the absorbance (Figure 3b,c). We then focused on the wavenumber ranges of 3412−3250 cm^{-1} (Figure 3d) and 1600−1300 cm^{-1} (Figure 3e), highlighting the peaks[128] corresponding to O−H (3330 cm^{-1})

https://doi.org/10.1021/acs.est.4c05782
Environ. Sci. Technol. XXXX, XXX, XXX−XXX

and C−O−H (1425 cm^{-1}). The peak intensities remained relatively low at temperatures up to 500 °C, but exhibited a significant increase at 550 °C and peaked at 650 °C (Figure 3g), suggesting the thermal degradation of K-PFOS within this temperature range. A previous study revealed that K-PFOS begins to melt at approximately 280 °C, and the molecules subsequently vaporize above this temperature, reaching maximum vaporization rates around 430 °C.[39] The observed changes in peak intensities (Figure 3d−g) align with the thermal phase transition stages of K-PFOS,[39] indicating that the formation of PIDs was mainly due to the decomposition of vapor phase of K-PFOS.

The thermal degradation mechanisms of PFAS, such as PFOA and PFOS, are not yet fully understood. Only a few studies have developed mechanisms based on experimental evidence. Wang et al. suggested direct F elimination from PFCAs during thermal treatments.[79] Blotevogel et al. found that the primary decomposition mechanism of PFOA is C−COOH cleavage, whereas α-elimination predominates in the breakdown of hexafluoropropylene oxide dimer acid (HFPO−DA).[48] Using density functional theory, Adi and Altarawneh explored various potential thermal decomposition pathways for HFPO−DA.[131] Additionally, Alinezhad et al.[42] and Sasi et al.[43] have investigated the thermal degradation mechanisms of PFCAs, HFPO−DA, and the long-chain homologues of HFPO−DA. The DFT computations[49] have illustrated that direct C−C β bond fission is thermodynamically (162 kJ/mol) preferred over fission of the terminal C−C bond forming CF_2 (232 kJ/mol) or elimination of an F atom (245 kJ/mol) producing perfluorinated alkenes. The findings from the present work, along with those of these previous studies,[42,43,48,49,79] collectively indicate that the initial homolytic cleavage or HF elimination reactions in parent PFAS leads to the formation of perfluoroalkyl radicals (eq 2), which then transform into organofluorine PIDs, including perfluoroalkenes (eqs 3 and 4).[43,44,51,57,132]

$$\mathrm{PFAS}(C_nF_{2n+1}-X)(g) \rightarrow C_nF_{2n+1}\bullet + X\bullet \quad (2)$$

$$C_nF_{2n+1}\bullet \rightarrow R_1-CF_2\bullet + R_2-CF = CF_2(\text{homolytic cleavage}) \quad (3)$$

$$C_nF_{2n+1}\bullet \rightarrow C_{n-2}F_{2n-3}-CF=CF_2 + F\bullet(\beta\text{elimination}) \quad (4)$$

This mechanism (eqs 2−4) is supported by the observed formation of perfluoropropene ($CF_3(FC{=}CF_2)$) from perfluorobutanoic acid ($CF_3(CF_2)_2COOH$), perfluoro-1-butene ($C_2F_5(FC{=}CF_2)$) from perfluoropentanoic acid ($CF_3(CF_2)_3COOH$), perfluoro(propyl vinyl ether) (C_3F_7O-$(FC{=}CF_2)$) from HPFO−DA ($C_3F_7OFCCF_3COOH$), and perfluorohept-1-ene ($C_5F_{11}(FC{=}CF_2)$) from both PFOA and PFOS.[42,51,86] In an oxygen-rich environment, the formed perfluoroalkyl radicals react with O_2 to form oxygen-containing products as observed in this study (Figures 2 and 3).

Different Catalysts/Additives. The thermal degradation of PFAS produces organofluorine PIDs and inorganic F species (Figures 1−3). Our investigation then progressed to examining approaches to reducing the generation of PIDs or maximizing the mineralization or the yield of inorganic F from PFAS through the amendment of cost-effective solid materials. Two previous studies have shown that the mineralization of PFCAs can be changed by dimethyl sulfoxide[87] and pure Pt.[79] Considering the high cost of pure Pt (~US$1000 per oz) and the potential for explosive reactions when dimethyl sulfoxide is mixed with certain compounds, we sought alternative materials. To this end, we evaluated biochar, GAC, and commercially available materials used in cracking and hydrogenation processes.[92−103]

As illustrated in Figure 4a, biochar failed to enhance the mineralization of PFOA. In contrast, GAC samples, particularly those from bituminous coal (F200 and Norit 400), dramatically boosted the $F_{yield,app}$ of PFOA from 6.5% to between 73 and 75% when heated at 300 °C (Figure 4a). HD4000, derived from lignite coal, also enhanced $F_{yield,app}$, though its effectiveness was less pronounced than that of the bituminous coal-based GACs. The enhanced mineralization of PFOA (vapor) at 150 °C and above may be attributed to its adsorption to GAC, which possesses a higher thermal conductivity than air.[134,135] While PFAS typically degrade in the gas phase in the absence of GAC, the presence of GAC may facilitate adsorption-enhanced or surface-mediated degradation processes. The exact mechanism of surface-assisted mineralization remains unclear and could be influenced by various factors, including the potential acceleration of initial cleavage steps. In contrast, biochar exhibits a significantly lower adsorption capacity for PFOA, previously measured at less than 30 L/kg[43] compared to >500 L/kg for GAC, indicating a less effective role in PFOA degradation.

A few mineral-based materials, such as Pt/Al_2O_3 and Pd/Al_2O_3, moderately increased $F_{yield,app}$ of PFOA. It is important to note that F radicals released from PFOA during the heating treatment may bind with the surfaces of some minerals, as previously observed by Wang et al.,[133] Alinezhad et al.,[51] and Abou-Khalil et al.,[90] resulting in an unextractable fraction of F. Nevertheless, the substantial increase in measurable $F_{yield,app}$ from PFOA in the presence of GAC clearly demonstrates its effectiveness and the advantages of using GAC in this application. The pressure inside a 300 mL sealed vessel when heated to 300 °C was estimated to be 1.9 atm or 0.2 MPa using the ideal gas law equation.

As illustrated in contour maps (Figure 4b,c), the addition of GAC significantly enhanced $F_{yield,app}$ from both PFOA and PFNA, peaking at 60−80% within temperatures of 300−400 °C after heating for 30- or 60 min. Figure 4d displays $F_{yield,app}$ values from four PFCAs at different temperatures during a 60 min treatment with GAC (F200). The results consistently show high yields of F achieved at 300 °C across all PFCAs studied.

Figure 4e gives the yield of F from PFOA when heated at 300 °C for 60 min in the presence of GAC across three consecutive cycles. The yield of F remained relatively consistent across the cycles, demonstrating the effectiveness of GAC in enhancing the thermal mineralization of PFOA. Additionally, the minimal decrease in GAC weight during these repeated uses further underscores its robustness for this purpose (Figure 4e). Interestingly, the yield of F from PFOA was slightly increased to >90% when heated with the reused GAC (Figure 4e).

Figure 5 provides further insights into the effects of various catalysts and additives on the PIDs formed from PFOA heated at 200−700 °C in air (Figure 5a−d) and N_2 (Figure 5e−h). With GAC, even at a lower temperature of 200 °C, we saw a significant reduction in PID peaks and the emergence of $(HF)_n$ peaks between 4000 and 3500 cm^{-1} (Figures 2b and 5a). The use of biochar also reduced the generation of PIDs; however,

https://doi.org/10.1021/acs.est.4c05782
Environ. Sci. Technol. XXXX, XXX, XXX−XXX

its impact on mineralization was much less pronounced (Figure 5b). The effectiveness of silica−alumina became apparent only at >500 °C, as indicated by the $(HF)_n$ peaks (Figure 5c). The porous, noncarbonaceous XAD-2 polymer did not enhance the mineralization of PFOA since $(HF)_n$ peaks were not observed in the spectra (Figure 5d).

In the inert N_2 atmosphere, the inclusion of GAC also enhanced the mineralization of PFOA (Figure 5e,f), evidenced by the appearance of the $(HF)_n$ peaks, analogous to observations made in the presence of GAC in air. These observations indicate that GAC is effective in both air and N_2 environments. Pd/Al_2O_3 (Figure 5g) appears to be an effective catalyst for PFOA mineralization, demonstrating a significant enhancement in $(HF)_n$ peaks similar to that observed with GAC. In contrast, Pt/Al_2O_3 (Figure 5h) was less efficient, which aligns with the F yields (Figure 4).

SiF_4 peak at ~1030 cm^{-1} was observed when PFOA was heated together with GAC in both air and N_2 atmospheres (Figure 5a,f). Wang et al. found that PFOA, when pyrolyzed on GAC, likely underwent mineralization into SiF_4, indicating that GAC enhances the conversion of PFOA into simpler inorganic forms.[136] This finding suggests that the presence of GAC can significantly influence the pathway and efficiency of PFOA's thermal decomposition, thereby facilitating more effective mineralization of PFOA.[136]

Enhanced Mineralization of PFNA, PFDA, Cationic PFAS, and K-PFOS. PFNA (Figure S25), PFDA (Figure S26), a cationic PFAS (Figure 6), and K-PFOS (Figure 7)

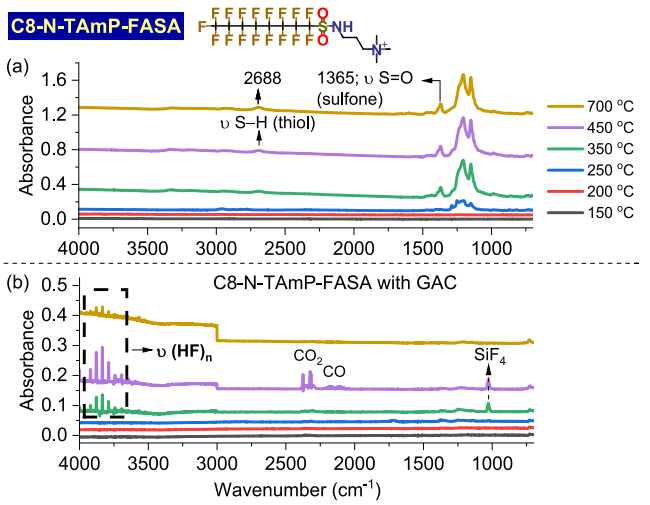

Figure 6. FTIR spectra of C8−N-TAmP-FASA heated in air: (a) without GAC and (b) with GAC. To enhance clarity, we have amplified the peak absorbance values between 4000 and 3000 cm^{-1} 5-fold in panel (b). The assignments of FTIR peaks for all PFAS analyzed in this study are detailed in Table S2.

were included to determine if the effects observed with GAC can be generalized across PFAS of different chain lengths and functionalities. The melting and boiling points of PFDA are higher than those of PFOA; the empirical evaporation point of melted PFDA is approximately 180 °C,[39] leading to the detection of gaseous phase PFDA at 200 °C, but not at 150 °C (Figure S26a). In the absence of GAC, the spectra reveal multiple peaks between 1800 and 1150 cm^{-1} (Figure S26a). In the presence of GAC, these peaks were significantly reduced, with a noticeable emergence of peaks of $(HF)_n$ between 4000 and 3500 cm^{-1}, indicating enhanced mineralization of PFDA (Figures 4d and S26b). Similar trends were observed for PFNA (Figure S25). Additionally, the emergence of the new peak at ~1723 cm^{-1} ($\nu C{=}C$) (Figures S25b and S26b) could signify the formation of perfluoro-2-alkene, such as perfluorooctene-2 (C_8F_{16}) (Figure S24).

C8-N-TAmP-FASA, an AFFF-relevant cationic polyfluoroalkyl substance (or precursor[57,117]), melts and vaporizes at higher temperatures than PFDA;[39] therefore, gas-phase C8-N-TAmP-FASA was not detected at temperatures below 250 °C (Figure 6a). With the presence of GAC, a significant reduction in peaks related to PIDs was observed (Figure 6b), coupled with an increase in the peaks for $(HF)_n$, demonstrating GAC's role in facilitating the mineralization of this compound as well.

The thermal mineralization of K-PFOS was also enhanced by GAC. Analyzing results from Figures S23 and 7a, we can see that introducing GAC significantly reduced or eliminated the absorption peaks associated with PIDs of K-PFOS heated in N_2 at temperatures above 500 °C, while peaks for $(HF)_n$ became apparent. This pattern was consistent when K-PFOS was heated with GAC in an air atmosphere, resulting in the disappearance of PID bands, particularly the peaks of CF_2O (Figures 3a and 7b). This suggests that GAC effectively aids in the thermal breakdown of K-PFOS, providing valuable insights into its potential application in both anaerobic and aerobic settings for environmental cleanup.

Note that in this study, pure PFAS were heated alongside GAC, rather than being preadsorbed onto it. The thermal behaviors of pure PFAS (e.g., K-PFOS) may differ from that of ionized species (e.g., PFOS anions). Nonetheless, the onset temperatures observed in this study—150 °C for PFOA heated with GAC and over 150 °C for PFOA heated alone—align with our previous findings[44] on the thermal treatment of PFAS preadsorbed on GAC.

The profound impact of GAC on the thermal degradation of PFAS support the following mechanism:[39] upon heating, crystalline PFAS solids melt into a liquid and then vaporize into a gas, and the thermal degradation of PFAS occurs primarily in the gas phase as PFAS vapor. The presence of GAC adsorbs PFAS vapor and promotes the degradation and mineralization through mechanisms that are under evaluation.[43,136]

Finally, because the peak at 1250 cm^{-1} is typical for both PFCs and HFCs (Figure 1b−d), the detection of a peak at 1250 cm^{-1} (e.g., Figures 2, 3, 5−7) cannot be used to substantiate the formation of CF_4. The peak at 1250 cm^{-1} is observed when PFAS are heated at low to moderate temperatures (Figures 2, 3, 5−7), suggesting the presence of non-CF_4 PFCs and HFCs, such as long-chain perfluoroalkenes identified through non-FTIR methods.[84−86] At temperatures above 300 or 400 °C, these compounds decompose into smaller PFCs and HFCs, with dominant absorbances shifting to around 1210 and 1150 cm^{-1} (Figure 1b,c), confirming that they are not CF_4, which has a single FTIR absorbance at around 1250 cm^{-1} and requires temperatures exceeding 1000 °C to decompose.[137] Recent studies have shown that long-chain perfluoroalkenes (e.g., perfluorohept-1-ene, C_7F_{14}) and perfluoroalkanes (e.g., perfluoro-*n*-heptane, C_7F_{16}) begin to decompose at temperatures 200 and 500 °C, respectively.[85,132]

■ ENVIRONMENTAL IMPLICATIONS

This study critically evaluates the formation of PIDs during the thermal treatment of five PFAS, including three that are newly

https://doi.org/10.1021/acs.est.4c05782
Environ. Sci. Technol. XXXX, XXX, XXX−XXX

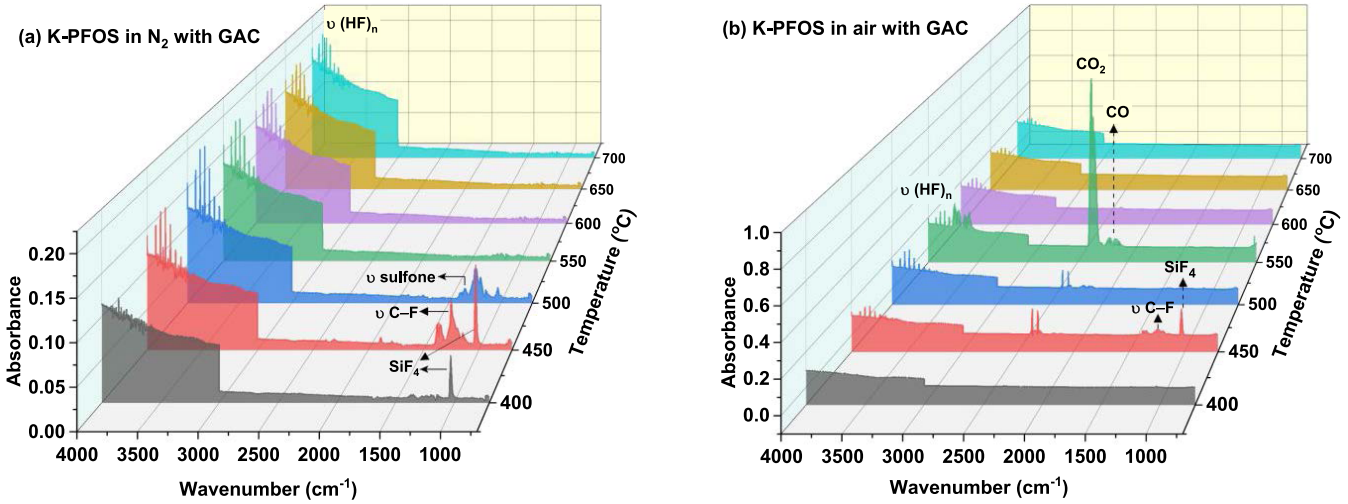

Figure 7. FTIR spectra of K-PFOS subjected to thermal treatment in the presence of GAC in (a) N_2 and (b) air atmospheres at varying temperatures. The peak absorbance values between 4000 and 3000 cm^{-1} have been amplified 5-fold to highlight $(HF)_n$ clusters.

regulated in drinking water.[27] For the first time, spectroscopic evidence is provided for the PIDs of PFNA, PFDA, and C8-N-TAmP-FASA. Under our experimental conditions, we found no evidence of CF_4 generation and observed that CF_2O formation is limited to narrow temperature ranges, specifically around 450 and 500 °C, when K-PFOS is heated in air without GAC.

Nevertheless, our data unveil the formation of PIDs from PFAS even at an elevated temperature of 700 °C (e.g., Figure 2), underscoring the challenges inherent in achieving complete PFAS mineralization. Hence, the second segment of this research, which centers on the identification of durable and cost-effective catalysts/additives that minimize PID generation from PFAS while optimizing mineralization, holds relevance for field thermal treatment research. Certain materials exhibited moderate effectiveness (e.g., Pd/Al_2O_3 and silica–alumina) (Figures 4 and 5), while GAC was found to be a robust and durable material that can minimize PID formation from various types of PFAS while improving the mineralization or defluorination of PFAS (Figures 4–7).

Overall, it is envisaged that the discoveries and insights from this study will deepen our understanding of PFAS thermal degradation and aid in the broader efforts to improve the cost-effectiveness and sustainability of PFAS remediation practices.

■ ASSOCIATED CONTENT

Supporting Information

The Supporting Information is available free of charge at https://pubs.acs.org/doi/10.1021/acs.est.4c05782.

Information includes PFAS included in this study, catalysts and additives, TGA–FTIR details, previous studies on PIDs of PFAS, PFAS included in the analysis (Table S1); FTIR peak assignments and conditions observed in this study (Table S2); TGA curves of a PFAS-free control (F200 GAC) (Figure S1); FTIR spectrum of PFOA at 150 °C in N_2 compared with the NIST reference (Figure S2); FTIR spectra of K-PFOS at 500 °C in air versus NIST references for CO and CO_2 (Figure S3); TGA curves of PFOA in N_2 (Figure S4); TGA curves of mixture of PFOA and GAC in N_2 (Figure S5); TGA curves of a mixture of PFOA and Pd/Al_2O_3 in N_2 (Figure S6); TGA curves of a mixture of PFOA and Pt/Al_2O_3 in N_2 (Figure S7); TGA curves of K-PFOS in N_2 (Figure S8); TGA curves of a mixture of K-PFOS and GAC in N_2 (Figure S9); TGA curves of PFOA in air (Figure S10); TGA curves of a mixture of PFOA and GAC in air (Figure S11); TGA curves of a mixture of PFOA and biochar in air (Figure S12); TGA curves of a mixture of PFOA and Si-alumina in air (Figure S13); TGA curves of a mixture of PFOA and XAD-2 resin beads in air (Figure S14); TGA curves of K-PFOS in air (Figure S15); TGA cures of a mixture of K-PFOS an GAC in air (Figure S16); TGA curves of C8-N-TAmP-FASA in air (Figure S17); TGA curves of a mixture of C8-N-TAmP-FASA and GAC in air (Figure S18); TGA curves of PFNA in air (Figure S19); TGA curves of a mixture of PFNA and GAC in air (Figure S20); TGA curves of PFDA in air (Figure S21); TGA curves of a mixture of PFDA and GAC in air (Figure S22); FTIR spectra of K-PFOS heated in N_2 (Figure S23); FTIR spectra of select PFCs highlighting absorbance at 1720 cm^{-1} (Figure S24); FTIR spectra of PFNA heated in air (Figure S25); and FTIR spectra of PFDA heated in air (Figure S26) (PDF)

■ AUTHOR INFORMATION

Corresponding Author

Feng Xiao − *Department of Civil and Environmental Engineering, The University of Missouri, Columbia, Missouri 65211, United States; Missouri Water Center, University of Missouri, Columbia, Missouri 65211, United States;* orcid.org/0000-0001-5686-6055; Phone: +1-573-882-0107; Email: Feng.Xiao@Missouri.edu, fxiaoee@gmail.com

Authors

Runze Sun − *Department of Civil and Environmental Engineering, The University of Missouri, Columbia, Missouri 65211, United States*

Ali Alinezhad − *Department of Civil and Environmental Engineering, The University of Missouri, Columbia, Missouri 65211, United States*

Mohammednoor Altarawneh − *Department of Chemical and Petroleum Engineering, United Arab Emirates University, Al-*

https://doi.org/10.1021/acs.est.4c05782
Environ. Sci. Technol. XXXX, XXX, XXX−XXX

Ain 15551, United Arab Emirates; orcid.org/0000-0002-2832-3886

Mohamed Ateia − *Department of Chemical and Biomolecular Engineering, Rice University, Houston, Texas 77005, United States;* orcid.org/0000-0002-3524-5513

Jens Blotevogel − *Commonwealth Scientific and Industrial Research Organisation (CSIRO), Environment, Waite Campus, Urrbrae 5064, Australia;* orcid.org/0000-0002-2740-836X

Jiamin Mai − *Department of Civil and Environmental Engineering, The University of Missouri, Columbia, Missouri 65211, United States*

Ravi Naidu − *Global Centre for Environmental Remediation (GCER), University of Newcastle, Callaghan 2308, Australia;* orcid.org/0000-0001-5529-8690

Joseph Pignatello − *Department of Environmental Sciences and Forestry, The Connecticut Agricultural Experiment Station, New Haven, Connecticut 06511, United States;* orcid.org/0000-0002-2772-5250

Anthony Rappe − *Department of Chemistry Colorado State University, Fort Collins, Colorado 80523, United States;* orcid.org/0000-0002-5259-1186

Xuejia Zhang − *Department of Civil and Environmental Engineering, The University of Missouri, Columbia, Missouri 65211, United States*

Complete contact information is available at: https://pubs.acs.org/10.1021/acs.est.4c05782

Author Contributions

R.S. performed research and contributed to data visualization. A.A. measured *F* yields of PFAS. M. Altarawneh, M. Ateia, J.B., J.M., R.N., J.P., and A.R. contributed to manuscript preparation. F.X. contributed to overall conception and design of the study, experimental design, data visualization, and manuscript drafting.

Notes

The authors declare no competing financial interest.

■ ACKNOWLEDGMENTS

This manuscript development was supported by the U.S. Department of Defense SERDP (ER22-4014), Environmental Research & Education Foundation, and U.S. National Science Foundation CAREER Program (2320966).

■ REFERENCES

(1) Prevedouros, K.; Cousins, I. T.; Buck, R. C.; Korzeniowski, S. H. Sources, fate and transport of perfluorocarboxylates. *Environ. Sci. Technol.* **2006**, *40* (1), 32−44.

(2) Buck, R. C.; Franklin, J.; Berger, U.; Conder, J. M.; Cousins, I. T.; de Voogt, P.; Jensen, A. A.; Kannan, K.; Mabury, S. A.; van Leeuwen, S. P. Perfluoroalkyl and polyfluoroalkyl substances in the environment: Terminology, classification, and origins. *Integr Environ. Assess Manage.* **2011**, *7* (4), 513−541.

(3) Evich, M. G.; Davis, M. J. B.; McCord, J. P.; Acrey, B.; Awkerman, J. A.; Knappe, D. R. U.; Lindstrom, A. B.; Speth, T. F.; Tebes-Stevens, C.; Strynar, M. J.; Wang, Z. Y.; Weber, E. J.; Henderson, W. M.; Washington, J. W. Per- and polyfluoroalkyl substances in the environment. *Science* **2022**, *375* (6580), No. eabg9065.

(4) Song, D.; Qiao, B.; Yao, Y.; Zhao, L.; Wang, X.; Chen, H.; Zhu, L.; Sun, H. Target and nontarget analysis of per- and polyfluoroalkyl substances in surface water, groundwater and sediments of three typical fluorochemical industrial parks in China. *J. Hazard Mater.* **2023**, *460*, No. 132411.

(5) Wang, Q.; Ruan, Y. F.; Yuen, C. N. T.; Lin, H. J.; Yeung, L. W. Y.; Leung, K. M. Y.; Lam, P. K. S. Tracing per- and polyfluoroalkyl substances (PFASs) in the aquatic environment: Target analysis and beyond. *TrAC, Trends Anal. Chem.* **2023**, *169*, No. 117351.

(6) Wang, T.; Vestergren, R.; Herzke, D.; Yu, J.; Cousins, I. T. Levels, isomer profiles, and estimated riverine mass discharges of perfluoroalkyl acids and fluorinated alternatives at the mouths of Chinese rivers. *Environ. Sci. Technol.* **2016**, *50* (21), 11584−11592.

(7) Pike, K. A.; Edmiston, P. L.; Morrison, J. J.; Faust, J. A. Correlation Analysis of Perfluoroalkyl Substances in Regional U.S. Precipitation Events. *Water Res.* **2021**, *190*, No. 116685.

(8) Kim, Y.; Pike, K. A.; Gray, R.; Sprankle, J. W.; Faust, J. A.; Edmiston, P. L. Non-targeted identification and semi-quantitation of emerging per- and polyfluoroalkyl substances (PFAS) in US rainwater. *Environ. Sci. Process Impacts* **2023**, *25* (11), 1771−1787.

(9) Mahmoud, M. A.; Karrman, A.; Oono, S.; Harada, K. H.; Koizumi, A. Polyfluorinated telomers in precipitation and surface water in an urban area of Japan. *Chemosphere* **2009**, *74* (3), 467−472.

(10) Scott, B. F.; Spencer, C.; Mabury, S. A.; Muir, D. C. G. Poly and perfluorinated carboxylates in north American precipitation. *Environ. Sci. Technol.* **2006**, *40* (23), 7167−7174.

(11) Xiao, F.; Halbach, T. R.; Simcik, M. F.; Gulliver, J. S. Input characterization of perfluoroalkyl substances in wastewater treatment plants: Source discrimination by exploratory data analysis. *Water Res.* **2012**, *46* (9), 3101−3109.

(12) Islam, M.; Thompson, K.; Dickenson, E.; Quiñones, O.; Steinle-Darling, E.; Westerhoff, P. Sucralose and Predicted De Facto Wastewater Reuse Levels Correlate with PFAS Levels in Surface Waters. *Environ. Sci. Technol. Lett.* **2023**, *10* (5), 431−438.

(13) Houtz, E. F.; Sutton, R.; Park, J. S.; Sedlak, M. Poly- and perfluoroalkyl substances in wastewater: Significance of unknown precursors, manufacturing shifts, and likely AFFF impacts. *Water Res.* **2016**, *95*, 142−149.

(14) Wanzek, T. A.; Field, J. A.; Kostarelos, K. Repeated Aqueous Film-Forming Foams Applications: Impacts on Polyfluoroalkyl Substances Retention in Saturated Soil. *Environ. Sci. Technol.* **2024**, *58* (3), 1659−1668.

(15) Davis, M. J. B.; Evich, M. G.; Goodrow, S. M.; Washington, J. W. Environmental Fate of Cl-PFPECAs: Accumulation of Novel and Legacy Perfluoroalkyl Compounds in Real-World Vegetation and Subsoils. *Environ. Sci. Technol.* **2023**, *57* (24), 8994−9004.

(16) Xiao, F.; Simcik, M. F.; Halbach, T. R.; Gulliver, J. S. Perfluorooctane sulfonate (PFOS) and perfluorooctanoate (PFOA) in soils and groundwater of a U.S. metropolitan area: Migration and implications for human exposure. *Water Res.* **2015**, *72*, 64−74.

(17) Zhou, T.; Li, X.; Liu, H.; Dong, S.; Zhang, Z.; Wang, Z.; Li, J.; Nghiem, L. D.; Khan, S. J.; Wang, Q. Occurrence, fate, and remediation for per-and polyfluoroalkyl substances (PFAS) in sewage sludge: A comprehensive review. *J. Hazard Mater.* **2024**, *466*, No. 133637.

(18) Ghaznavi, S. M.; Zimmerman, C.; Shea, M. E.; MacRae, J. D.; Peckenham, J. M.; Noblet, C. L.; Apul, O. G.; Kopec, A. D. Management of per- and polyfluoroalkyl substances (PFAS)-laden wastewater sludge in Maine: Perspectives on a wicked problem. *Biointerphases* **2023**, *18* (4), No. 041004.

(19) Link, G. W.; Reeves, D. M.; Cassidy, D. P.; Coffin, E. S. Per- and polyfluoroalkyl substances (PFAS) in final treated solids (Biosolids) from 190 Michigan wastewater treatment plants. *J. Hazard. Mater.* **2024**, *463*, No. 132734.

(20) Liu, Z. Y.; Liu, S.; Xiao, F.; Sweetman, A. J.; Cui, Q. Q.; Guo, H.; Xu, J. Y.; Luo, Z. Y.; Wang, M. X.; Zhong, L. L.; Gan, J. Y.; Tan, W. F. Tissue-specific distribution and bioaccumulation of perfluoroalkyl acids, isomers, alternatives, and precursors in citrus trees of contaminated fields: Implication for risk assessment. *J. Hazard. Mater.* **2024**, *465*, No. 133184.

(21) Costello, M. C. S.; Lee, L. S. Sources, Fate, and Plant Uptake in Agricultural Systems of Per- and Polyfluoroalkyl Substances. *Curr. Pollut. Rep.* **2024**, *10*, 799−819.

(22) Zhang, J. C.; Li, W.; Yang, L. P.; Chu, Z. H.; Jiao, Y. N.; Wang, L.; Zhu, L. J.; Qin, C. A.; Liu, R.; Gao, X. B. Legacy per- and polyfluoroalkyl substances (PFASs) especially alternative PFASs in shellfish from Shandong Province, China: Distribution, sources, and health risk. *Mar. Pollut. Bull.* **2023**, *195*, No. 115465.
(23) Chu, S.; Letcher, R. J. A targeted and non-targeted discovery screening approach for poly-and per-fluoroalkyl substances in model environmental biota samples. *J. Chromatogr. A* **2024**, *1715*, No. 464584.
(24) Barrett, H.; Du, X.; Houde, M.; Lair, S.; Verreault, J.; Peng, H. Suspect and nontarget screening revealed class-specific temporal trends (2000−2017) of poly- and perfluoroalkyl substances in St. Lawrence Beluga whales. *Environ. Sci. Technol.* **2021**, *55* (3), 1659−1671.
(25) Yi, S. J.; Zhu, L. Y.; Mabury, S. A. First report on in vivo pharmacokinetics and biotransformation of chlorinated polyfluoroalkyl ether sulfonates in rainbow trout. *Environ. Sci. Technol.* **2020**, *54* (1), 345−354.
(26) Li, Y. N.; Yao, J. Z.; Zhang, J.; Pan, Y. T.; Dai, J. Y.; Ji, C. L.; Tang, J. H. First Report on the Bioaccumulation and Trophic Transfer of Perfluoroalkyl Ether Carboxylic Acids in Estuarine Food Web. *Environ. Sci. Technol.* **2022**, *56* (10), 6046−6055.
(27) USEPA. Final PFAS National Primary Drinking Water Regulation 2024 https://www.epa.gov/sdwa/and-polyfluoroalkyl-substances-pfas. (accessed April 2024).
(28) USEPA. Designation of PFOA and PFOS as hazardous substances under CERCLA Release Reporting Requirements Factsheet 2024 https://www.epa.gov/epcra/designation-pfoa-and-pfos-hazardous-substances-under-cercla-release-reporting-requirements. (accessed April 2024).
(29) Juve, J. M. A.; Reece, J. A. D.; Wong, M. S.; Wei, Z. S.; Ateia, M. Photocatalysts for chemical-free PFOA degradation - What we know and where we go from here? *J. Hazard. Mater.* **2024**, *462*, No. 132651.
(30) Umeh, A. C.; Stegh, J.; Naidu, R. Toward In Situ Sequestration of Multicomponent PFAS Using Injectable Adsorbent Suspensions. *ACS ES&T Water* **2023**, *3* (12), 3858−3873.
(31) Li, C.; Shen, C.; Gao, B.; Liang, W.; Zhu, Y.; Shi, W.; Ai, S.; Xu, H.; Wu, J.; Sun, Y. Degradation and mechanism of PFOA by peroxymonosulfate activated by nitrogen-doped carbon foam-anchored nZVI in aqueous solutions. *Chemosphere* **2024**, *351*, No. 141209.
(32) Serna-Sanchez, E.; Pellizzeri, S. Predicting pyrolysis decomposition of PFOA using computational nanoreactors: a thermodynamic study. *RSC Adv.* **2023**, *13* (37), 25699−25703.
(33) Weber, N. H.; Grimison, C. C.; Lucas, J. A.; Mackie, J. C.; Stockenhuber, M.; Kennedy, E. M. Influence of reactor composition on the thermal decomposition of perfluorooctanesulfonic acid (PFOS). *J. Hazard. Mater.* **2024**, *461*, No. 132665.
(34) Vatankhah, H.; Anderson, R. H.; Ghosh, R.; Willey, J.; Leeson, A. A review of innovative approaches for onsite management of PFAS-impacted investigation derived waste. *Water Res.* **2023**, *247*, No. 120769.
(35) Mitov, S.; Panchenko, A.; Roduner, E. Comparative DFT study of non-fluorinated and perfluorinated alkyl and alkyl-peroxy radicals. *Chem. Phys. Lett.* **2005**, *402* (4−6), 485−490.
(36) Ellis, D. A.; Mabury, S. A.; Martin, J. W.; Muir, D. C. G. Thermolysis of fluoropolymers as a potential source of halogenated organic acids in the environment. *Nature* **2001**, *412* (6844), 321−324.
(37) Xiao, F.; Deng, B.; Dionysiou, D. D.; Karanfil, T.; O'Shea, K.; Roccaro, P.; Xiong, Z. J.; Zhao, D. Cross-national challenges and strategies for PFAS regulatory compliance in water infrastructure. *Nature Water* **2023**, *1*, 1004−1015.
(38) USEPA. PFAS National Primary Drinking Water Regulation Rulemaking 2023 https://www.epa.gov/system/files/documents/-03/Pre-Publication%20Federal%20Register%20Notice_PFAS%20NPDWR_NPRM_Final_3.13.23.pdf. (accessed March 15, 2023).
(39) Xiao, F.; Sasi, P. C.; Alinezhad, A.; Sun, R.; Abdulmalik Ali, M. Thermal Phase Transition and Rapid Degradation of Forever Chemicals (PFAS) in Spent Media Using Induction Heating. *ACS ES&T Eng.* **2023**, *3* (9), 1370−1380.
(40) Wang, Z.; Alinezhad, A.; Sun, R.; Xiao, F.; Pignatello, J. J. Pre- and Postapplication Thermal Treatment Strategies for Sorption Enhancement and Reactivation of Biochars for Removal of Per- and Polyfluoroalkyl Substances from Water. *ACS ES&T Eng.* **2023**, *3* (2), 193−200.
(41) Sun, R. Z.; Sasi, P. C.; Alinezhad, A.; Xiao, F. Sorptive removal of per- and polyfluoroalkyl substances (PFAS) in organic-free water, surface water, and landfill leachate and thermal reactivation of spent sorbents. *J. Hazard. Mater. Adv.* **2023**, *10*, No. 100311.
(42) Alinezhad, A.; Shao, H.; Litvanova, K.; Sun, R. Z.; Kubatova, A.; Zhang, W.; Li, Y.; Xiao, F. Mechanistic Investigations of Thermal Decomposition of Perfluoroalkyl Ether Carboxylic Acids and Short-Chain Perfluoroalkyl Carboxylic Acids. *Environ. Sci. Technol.* **2023**, *57* (23), 8796−8807.
(43) Sasi, P. C.; Alinezhad, A.; Yao, B.; Kubatova, A.; Golovko, S. A.; Golovko, M. Y.; Xiao, F. Effect of granular activated carbon and other porous materials on thermal decomposition of per- and polyfluoroalkyl substances: Mechanisms and implications for water purification. *Water Res.* **2021**, *200*, No. 117271.
(44) Xiao, F.; Sasi, P. C.; Yao, B.; Kubatova, A.; Golovko, S. A.; Golovko, M. Y.; Soli, D. Thermal stability and decomposition of perfluoroalkyl substances on spent granular activated carbon. *Environ. Sci. Technol. Lett.* **2020**, *7* (5), 343−350.
(45) Soker, O.; Hao, S. L.; Trewyn, B. G.; Higgins, C. P.; Strathmann, T. J. Application of Hydrothermal Alkaline Treatment to Spent Granular Activated Carbon: Destruction of Adsorbed PFASs and Adsorbent Regeneration. *Environ. Sci. Technol. Lett.* **2023**, *10* (5), 425−430.
(46) Zhang, Q.; Mian, M. M.; Zhang, A.; Zhou, L.; Du, R.; Ao, W.; Yu, G.; Deng, S. Catalytic Degradation of Hexafluoropropylene Oxide Trimeric Acid during the Hydrothermal Regeneration of Spent Activated Carbon. *ACS ES&T Eng.* **2024**, *4* (6), 1391−1400.
(47) Cornell, R. E.; Burke, M. P. Low-temperature oxidation pathways are critical to thermal incineration of PFAS-laden materials. *J. Hazard. Mater. Lett.* **2024**, *5*, No. 100100.
(48) Blotevogel, J.; Giraud, R. J.; Rappé, A. K. Incinerability of PFOA and HFPO-DA: Mechanisms, kinetics, and thermal stability ranking. *Chem. Eng. J.* **2023**, *457*, No. 141235.
(49) Altarawneh, M.; Almatarneh, M. H.; Dlugogorski, B. Z. Thermal decomposition of perfluorinated carboxylic acids: Kinetic model and theoretical requirements for PFAS incineration. *Chemosphere* **2022**, *286*, No. 131685.
(50) Dastgheib, S. A.; Mock, J.; Ilangovan, T.; Patterson, C. Thermogravimetric studies for the incineration of an anion exchange resin laden with short- or long-chain PFAS compounds containing carboxylic or sulfonic acid functionalities in the presence or absence of calcium oxide. *Ind. Eng. Chem. Res.* **2021**, *60* (47), 16961−16968.
(51) Alinezhad, A.; Sasi, P. C.; Zhang, P.; Yao, B.; Kubatova, A.; Golovko, S. A.; Golovko, M. Y.; Xiao, F. An investigation of thermal air degradation and pyrolysis of per- and polyfluoroalkyl substances and aqueous film-forming foams in soil. *ACS ES&T Eng.* **2022**, *2* (2), 198−209.
(52) Winchell, L. J.; Ross, J. J.; Wells, M. J. M.; Fonoll, X.; Norton, J. W.; Bell, K. Y. Per- and polyfluoroalkyl substances thermal destruction at water resource recovery facilities: A state of the science review. *Water Environ. Res.* **2021**, *93* (6), 826−843.
(53) Kundu, S.; Patel, S.; Halder, P.; Patel, T.; Marzbali, M. H.; Pramanik, B. K.; Paz-Ferreiro, J.; de Figueiredo, C. C.; Bergmann, D.; Surapaneni, A.; Megharaj, M.; Shah, K. Removal of PFASs from biosolids using a semi-pilot scale pyrolysis reactor and the application of biosolids derived biochar for the removal of PFASs from contaminated water. *Environ. Sci.: Water Res. Technol.* **2021**, *7*, 638−649.
(54) Thoma, E. D.; Wright, R. S.; George, I.; Krause, M.; Presezzi, D.; Villa, V.; Preston, W.; Deshmukh, P.; Kauppi, P.; Zemek, P. G.

https://doi.org/10.1021/acs.est.4c05782
Environ. Sci. Technol. XXXX, XXX, XXX−XXX

Pyrolysis processing of PFAS-impacted biosolids, a pilot study. *J. Air Waste Manage. Assoc.* **2022**, *72* (4), 309−318.
(55) Duchesne, A. L.; Brown, J. K.; Patch, D. J.; Major, D.; Weber, K. P.; Gerhard, J. I. Remediation of PFAS-contaminated soil and granular activated carbon by smoldering combustion. *Environ. Sci. Technol.* **2020**, *54* (19), 12631−12640.
(56) Fournie, T.; Rashwan, T. L.; Switzer, C.; Gerhard, J. I. Smouldering to treat PFAS in sewage sludge. *Waste Manage.* **2023**, *164*, 219−227.
(57) Xiao, F.; Sasi, P. C.; Alinezhad, A.; Golovko, S. A.; Golovko, M. Y.; Spoto, A. Thermal decomposition of anionic, awitterionic, and cationic polyfluoroalkyl substances in aqueous film-forming foams. *Environ. Sci. Technol.* **2021**, *55* (14), 9885−9894.
(58) Divine, C.; March, L.; Kalra, S. S.; Hurst, J. Sonolysis and Super Critical Water Oxidation (SCWO): Development Maturity and Potential for Destroying PFAS. *Groundwater Monit. Rem.* **2023**, *43*, 18−33.
(59) Shende, T.; Andaluri, G.; Suri, R. P. S. Kinetic model for sonolytic degradation of non-volatile surfactants: Perfluoroalkyl substances. *Ultrason. Sonochem.* **2019**, *51*, 359−368.
(60) Ilić, N.; Andalib, A.; Lippert, T.; Knoop, O.; Franke, M.; Bräutigam, P.; Drewes, J. E.; Huebner, U. Ultrasonic degradation of GenX (HFPO-DA)-Performance comparison to PFOA and PFOS at high frequencies. *Chem. Eng. J.* **2023**, *472*, No. 144630.
(61) Zhang, K.; Huang, J.; Yu, G.; Zhang, Q.; Deng, S.; Wang, B. Destruction of perfluorooctane sulfonate (PFOS) and perfluorooctanoic acid (PFOA) by ball milling. *Environ. Sci. Technol.* **2013**, *47* (12), 6471−6477.
(62) Turner, L. P.; Kueper, B. H.; Jaansalu, K. M.; Patch, D. J.; Battye, N.; El-Sharnouby, O.; Mumford, K. G.; Weber, K. P. Mechanochemical remediation of perfluorooctanesulfonic acid (PFOS) and perfluorooctanoic acid (PFOA) amended sand and aqueous film-forming foam (AFFF) impacted soil by planetary ball milling. *Sci. Total Environ.* **2021**, *765*, No. 142722.
(63) Yang, N. Y.; Yang, S. S.; Ma, Q. Q.; Beltran, C.; Guan, Y. Q.; Morsey, M.; Brown, E.; Fernando, S.; Holsen, T. M.; Zhang, W.; Yang, Y. Solvent-Free Nonthermal Destruction of PFAS Chemicals and PFAS in Sediment by Piezoelectric Ball Milling. *Environ. Sci. Technol. Lett.* **2023**, *10*, 198−203.
(64) Weber, N. H.; Stockenhuber, S. P.; Delva, C. S.; Fara, A. A.; Grimison, C. C.; Lucas, J. A.; Mackie, J. C.; Stockenhuber, M.; Kennedy, E. M. Kinetics of Decomposition of PFOS Relevant to Thermal Desorption Remediation of Soils. *Ind. Eng. Chem. Res.* **2021**, *60* (25), 9080−9087.
(65) Crownover, E.; Oberle, D.; Kluger, M.; Heron, G. Perfluoroalkyl and polyfluoroalkyl substances thermal desorption evaluation. *Biorem. J.* **2019**, *29* (4), 77−81.
(66) Sörengård, M.; Lindh, A. S.; Ahrens, L. Thermal desorption as a high removal remediation technique for soils contaminated with per- and polyfluoroalkyl substances (PFASs). *PLoS One* **2020**, *15* (6), e0234476 DOI: 10.1371/journal.pone.0234476.
(67) Saleem, M.; Biondo, O.; Sretenovic, G.; Tomei, G.; Magarotto, M.; Pavarin, D.; Marotta, E.; Paradisi, C. Comparative performance assessment of plasma reactors for the treatment of PFOA; reactor design, kinetics, mineralization and energy yield. *Chem. Eng. J.* **2020**, *382*, No. 123031.
(68) Singh, R. K.; Fernando, S.; Baygi, S. F.; Multari, N.; Thagard, S. M.; Holsen, T. M. Breakdown products from perfluorinated alkyl substances (PFAS) degradation in a plasma-based water treatment process. *Environ. Sci. Technol.* **2019**, *53* (5), 2731−2738.
(69) Fromme, H.; Wockner, M.; Roscher, E.; Volkel, W. ADONA and perfluoroalkylated substances in plasma samples of German blood donors living in South Germany. *Int. J. Hyg. Environ. Health* **2017**, *220*, 455−460.
(70) Hao, S.; Choi, Y. J.; Deeb, R. A.; Strathmann, T. J.; Higgins, C. P. Application of Hydrothermal Alkaline Treatment for Destruction of Per- and Polyfluoroalkyl Substances in Contaminated Groundwater and Soil. *Environ. Sci. Technol.* **2022**, *56* (10), 6647−6657.
(71) Zhang, W. L.; Liang, Y. N. Effects of hydrothermal treatments on destruction of per- and polyfluoroalkyl substances in sewage sludge. *Environ. Pollut.* **2021**, *285*, No. 117276.
(72) Li, J.; Pinkard, B. R.; Wang, S.; Novosselov, I. V. Review: Hydrothermal treatment of per- and polyfluoroalkyl substances (PFAS). *Chemosphere* **2022**, *307* (Pt 2), No. 135888.
(73) Hao, S.; Choi, Y. J.; Wu, B.; Higgins, C. P.; Deeb, R.; Strathmann, T. J. Hydrothermal alkaline treatment for destruction of per- and polyfluoroalkyl substances in aqueous film-forming foam. *Environ. Sci. Technol.* **2021**, *55* (5), 3283−3295.
(74) Li, J. N.; Austin, C.; Moore, S.; Pinkard, B. R.; Novosselov, I. V. PFOS destruction in a continuous supercritical water oxidation reactor. *Chem. Eng. J.* **2023**, *451*, No. 139063.
(75) Chiang, S.-Y.; Saba, M.; Leighton, M.; Ballenghien, D.; Hatler, D.; Gal, J.; Deshusses, M. A. Supercritical water oxidation for the destruction of spent media wastes generated from PFAS treatment. *J. Hazard. Mater.* **2023**, *460*, No. 132264.
(76) Krause, M. J.; Thoma, E.; Sahle-Damesessie, E.; Crone, B.; Whitehill, A.; Shields, E.; Gullett, B. Supercritical Water Oxidation as an Innovative Technology for PFAS Destruction. *J. Environ. Eng.* **2022**, *148* (2), 05021006.
(77) Pinkard, B. R.; Shetty, S.; Stritzinger, D.; Bellona, C.; Novosselov, I. V. Destruction of perfluorooctanesulfonate (PFOS) in a batch supercritical water oxidation reactor. *Chemosphere* **2021**, *279*, No. 130834.
(78) NIH. Carbonyl fluoride 2023 https://pubchem.ncbi.nlm.nih.gov/compound/Carbonyl-fluoride. (accessed October 2023).
(79) Wang, J.; Song, M.; Abusallout, I.; Hanigan, D. Thermal Decomposition of Two Gaseous Perfluorocarboxylic Acids: Products and Mechanisms. *Environ. Sci. Technol.* **2023**, *57* (15), 6179−6187.
(80) Weber, N. H.; Redfern, H.; Grimison, C. C.; Lucas, J. A.; Mackie, J. C.; Stockenhuber, M.; Kennedy, E. M. Formation of Products of Incomplete Destruction (PID) from the Thermal Oxidative Decomposition of Perfluorooctanoic Acid (PFOA): Measurement, Modeling, and Reaction Pathways. *J. Phys. Chem. A* **2024**, *128*, 5362−5373.
(81) Weber, N. H.; Delva, C. S.; Stockenhuber, S. P.; Grimison, C. C.; Lucas, J. A.; Mackie, J. C.; Stockenhuber, M.; Kennedy, E. M. Modeling and Experimental Study on the Thermal Decomposition of Perfluorooctanesulfonic Acid (PFOS) in an α-Alumina Reactor. *Ind. Eng. Chem. Res.* **2022**, *61* (16), 5453−5463.
(82) Weber, N. H.; Dixon, L. J.; Stockenhuber, S. P.; Grimison, C. C.; Lucas, J. A.; Mackie, J. C.; Mackie, J. C.; Stockenhuber, M.; Stockenhuber, M.; Kennedy, E. M. Thermal decomposition of PFOA: Influence of reactor and reaction conditions on product formation. *Chem. Eng. Sci.* **2023**, *278*, No. 118924.
(83) Hughey, K. D.; Gallagher, N. B.; Zhao, Y.; Thakur, N.; Bradley, A. M.; Koster van Groos, P. G.; Johnson, T. J. PFAS remediation: Evaluating the infrared spectra of complex gaseous mixtures to determine the efficacy of thermal decomposition of PFAS. *Chemosphere* **2024**, *362*, No. 142631.
(84) Shields, E. P.; Krug, J. D.; Roberson, W. R.; Jackson, S. R.; Smeltz, M. G.; Allen, M. R.; Burnette, R. P.; Nash, J. T.; Virtaranta, L.; Preston, W.; Liberatore, H. K.; Ariel Geer Wallace, M.; Ryan, J. V.; Kariher, P. H.; Lemieux, P. M.; Linak, W. P. Pilot-Scale Thermal Destruction of Per- and Polyfluoroalkyl Substances in a Legacy Aqueous Film Forming Foam. *ACS ES&T Eng.* **2023**, *3* (9), 1308−1317.
(85) Yao, B.; Sun, R.; Alinezhad, A.; Kubatova, A.; Simcik, M. F.; Guan, X.; Xiao, F. The first quantitative investigation of compounds generated from PFAS, PFAS-containing aqueous film-forming foams and commercial fluorosurfactants in pyrolytic processes. *J. Hazard. Mater.* **2022**, *436*, No. 129313.
(86) Krusic, P. J.; Roe, D. C. Gas-phase NMR technique for studying the thermolysis of materials: Thermal decomposition of ammonium perfluorooctanoate. *Anal. Chem.* **2004**, *76* (13), 3800−3803.
(87) Trang, B.; Li, Y.; Xue, X. S.; Ateia, M.; Houk, K. N.; Dichtel, W. R. Low-temperature mineralization of perfluorocarboxylic acids. *Science* **2022**, *377* (6608), 839−845.

(88) Riedel, T. P.; Wallace, M. A. G.; Shields, E. P.; Ryan, J. V.; Lee, C. W.; Linak, W. P. Low temperature thermal treatment of gas-phase fluorotelomer alcohols by calcium oxide. *Chemosphere* **2021**, *272*, No. 129859.
(89) Wang, F.; Lu, X.; Li, X. Y.; Shih, K. Effectiveness and mechanisms of defluorination of perfluorinated alkyl substances by calcium compounds during waste thermal treatment. *Environ. Sci. Technol.* **2015**, *49* (9), 5672−5680.
(90) Abou-Khalil, C.; Chernysheva, L.; Miller, A.; Abarca-Perez, A.; Peaslee, G.; Herckes, P.; Westerhoff, P.; Doudrick, K. Enhancing the Thermal Mineralization of Perfluorooctanesulfonate on Granular Activated Carbon Using Alkali and Alkaline-Earth Metal Additives. *Environ. Sci. Technol.* **2024**, *58* (25), 11162−11174.
(91) Shields, E. P.; Wallace, M. A. G. Low temperature destruction of gas-phase per- and polyfluoroalkyl substances using an alumina-based catalyst. *J. Air Waste Manage. Assoc.* **2023**, *73* (7), 525−532.
(92) Burch, R.; Loader, P. K. Investigation of Pt/Al2o3 and Pd/Al2o3 Catalysts for the Combustion of Methane at Low Concentrations. *Appl. Catal., B* **1994**, *5* (1−2), 149−164.
(93) Qian, W. H.; Shirai, H.; Ifuku, M.; Ishihara, A.; Kabe, T. Reactions of Tetralin with Tritiated Molecular Hydrogen on Pt/Al2O3, Pd/Al2O3, and Pt−Pd/Al2O3 Catalysts. *Energy Fuel* **2000**, *14* (6), 1205−1211.
(94) Doi, K.; Wu, Y. Y.; Takeda, R.; Matsunami, A.; Arai, N.; Tagawa, T.; Goto, S. Catalytic decomposition of N2O in medical operating rooms over Rh/Al2O3, Pd/Al2O3, and Pt/Al2O3. *Appl. Catal., B* **2001**, *35* (1), 43−51.
(95) Yorgun, S.; Simsek, Y. E. Catalytic pyrolysis of Miscanthus × giganteus over activated alumina. *Bioresour. Technol.* **2008**, *99* (17), 8095−8100.
(96) Leung, A.; Boocock, D. G. B.; Konar, S. K. Pathway for the Catalytic Conversion of Carboxylic-Acids to Hydrocarbons over Activated Alumina. *Energy Fuel* **1995**, *9* (5), 913−920.
(97) Vonghia, E.; Boocock, D. G. B.; Konar, S. K.; Leung, A. Pathways for the Deoxygenation of Triglycerides to Aliphatic-Hydrocarbons over Activated Alumina. *Energy Fuel* **1995**, *9* (6), 1090−1096.
(98) de Jong, K. P.; Zecevic, J.; Friedrich, H.; de Jongh, P. E.; Bulut, M.; van Donk, S.; Kenmogne, R.; Finiels, A.; Hulea, V.; Fajula, F. Zeolite Y Crystals with Trimodal Porosity as Ideal Hydrocracking Catalysts. *Angew. Chem., Int. Ed.* **2010**, *49* (52), 10074−10078.
(99) Qin, Z. X.; Shen, B. J.; Yu, Z. W.; Deng, F.; Zhao, L.; Zhou, S. G.; Yuan, D. L.; Gao, X. H.; Wang, B. J.; Zhao, H. J.; Liu, H. H. A defect-based strategy for the preparation of mesoporous zeolite Y for high-performance catalytic cracking. *J. Catal.* **2013**, *298*, 102−111.
(100) Corma, A.; Mocholi, F.; Orchilles, V.; Koermer, G. S.; Madon, R. J. Methylcyclohexane and Methylcyclohexene Cracking over Zeolite-Y Catalysts. *Appl. Catal.* **1990**, *67* (2), 307−324.
(101) Wang, Z.; Jiang, Y.; Baiker, A.; Huang, J. Pentacoordinated Aluminum Species: New Frontier for Tailoring Acidity-Enhanced Silica-Alumina Catalysts. *Acc. Chem. Res.* **2020**, *53* (11), 2648−2658.
(102) Coumans, A. E.; Poduval, D. G.; van Veen, J. A. R.; Hensen, E. J. M. The nature of the sulfur tolerance of amorphous silica-alumina supported NiMo(W) sulfide and Pt hydrogenation catalysts. *Appl. Catal., A* **2012**, *411-412*, 51−59.
(103) Arai, H.; Machida, M. Thermal stabilization of catalyst supports and their application to high-temperature catalytic combustion. *Appl. Catal., A* **1996**, *138* (2), 161−176.
(104) III, Insurance Information Institute (III). Wildfire statistics 2020 http://www.iii.org/fact-statistic/wildfires.
(105) Skjernstad, J.; Taylor, J. A.; Smernik, R. J. Estimation of charcoal (char) in soils. *Commun. Soil Sci. Plan* **1999**, *30* (15−16), 2283−2298.
(106) Lehmann, J.; Joseph, S. *Biochar for Environmental Management: Science and Technology*; Earthscan Publications Ltd.: London, UK, 2009; p 416.
(107) Schmidt, M. W. I.; Noack, A. G. Black carbon in soils and sediments: Analysis, distribution, implications, and current challenges. *Global Biogeochem. Cycles* **2000**, *14* (3), 777−793.
(108) Skjemstad, J. O.; Reicosky, D. C.; Wilts, A. R.; McGowan, J. A. Charcoal carbon in U.S. agricultural soils. *Soil Sci. Soc. Am. J.* **2002**, *66* (4), 1249−1255.
(109) Xiao, F.; Bedane, A. H.; Mallula, S.; Challa Sasi, P.; Alinezhad, A.; Soli, D.; Hagen, Z. M.; Mann, M. D. Production of granular activated carbon by thermal air oxidation of biomass charcoal/biochar for water treatment in rural communities: A mechanistic investigation. *Chem. Eng. J. Adv.* **2020**, *4*, No. 100035.
(110) Xiao, F.; Bedane, A. H.; Zhao, J. X.; Mann, M. D.; Pignatello, J. J. Thermal air oxidation changes surface and adsorptive properties of black carbon (char/biochar). *Sci. Total Environ.* **2018**, *618*, 276−283.
(111) Mao, J. D.; Johnson, R. L.; Lehmann, J.; Olk, D. C.; Neves, E. G.; Thompson, M. L.; Schmidt-Rohr, K. Abundant and stable char residues in soils: Implications for soil fertility and carbon sequestration. *Environ. Sci. Technol.* **2012**, *46* (17), 9571−9576.
(112) Glaser, B.; Haumaier, L.; Guggenberger, G.; Zech, W. The 'Terra Preta' phenomenon: A model for sustainable agriculture in the humid tropics. *Naturwissenschaften* **2001**, *88* (1), 37−41.
(113) Wu, C.; An, W.; Liu, Z.; Lin, J.; Qian, Z.; Xue, S. The effects of biochar as the electron shuttle on the ferrihydrite reduction and related arsenic (As) fate. *J. Hazard. Mater.* **2020**, *390*, No. 121391.
(114) Kappler, A.; Wuestner, M. L.; Ruecker, A.; Harter, J.; Halama, M.; Behrens, S. Biochar as an electron shuttle between bacteria and Fe(III) minerals. *Environ. Sci. Technol. Lett.* **2014**, *1* (8), 339−344.
(115) Zhou, G. W.; Yang, X. R.; Li, H.; Marshall, C. W.; Zheng, B. X.; Yan, Y.; Su, J. Q.; Zhu, Y. G. Electron Shuttles Enhance Anaerobic Ammonium Oxidation Coupled to Iron(III) Reduction. *Environ. Sci. Technol.* **2016**, *50* (17), 9298−9307.
(116) Barzen-Hanson, K. A.; Roberts, S. C.; Choyke, S.; Oetjen, K.; McAlees, A.; Riddell, N.; McCrindle, R.; Ferguson, P. L.; Higgins, C. P.; Field, J. A. Discovery of 40 classes of per- and polyfluoroalkyl substances in historical aqueous film-forming foams (AFFFs) and AFFF-impacted groundwater. *Environ. Sci. Technol.* **2017**, *51* (4), 2047−2057.
(117) Jin, B.; Mallula, S.; Golovko, S. A.; Golovko, M. Y.; Xiao, F. In vivo generation of PFOA, PFOS, and other compounds from cationic and zwitterionic per- and polyfluoroalkyl substances in a terrestrial invertebrate (Lumbricus terrestris). *Environ. Sci. Technol.* **2020**, *54* (12), 7378−7387.
(118) NIST. Carbonic Difluoride 2023 https://webbook.nist.gov/cgi/cbook.cgi?ID=C353504&Mask=80.
(119) SpectraBase. SiF4 Spectrum 2024 https://spectrabase.com/spectrum/4MiF42xszHd.
(120) Baker, T. J.; Tonkyn, R. G.; Thompson, C. J.; Dunlap, M. K.; van Groos, P. G. K.; Thakur, N. A.; Wilhelm, M. J.; Myers, T. L.; Johnson, T. J. An infrared spectral database for gas-phase quantitation of volatile per- and polyfluoroalkyl substances (PFAS). *J. Quant. Spectrosc. Radiat. Transfer* **2023**, *295*, No. 108420.
(121) NIST. Pentafluoro-ethane (C2HF5) 2023 https://webbook.nist.gov/cgi/cbook.cgi?ID=354-33-6&Type=IR-SPEC&Index=QUANT-IR,15.
(122) NIST. Tetrafluoromethane 2023 https://webbook.nist.gov/cgi/cbook.cgi?ID=C75730&Type=IR-SPEC&Index=0.
(123) NIST. Hxafluoro-ethane (C2F6) 2023 https://webbook.nist.gov/cgi/cbook.cgi?ID=76-16-4&Type=IR-SPEC&Index=QUANT-IR,0.
(124) NIST. Tetrafluoro-ethene (C2F4) 2023 https://webbook.nist.gov/cgi/cbook.cgi?ID=C116143&Type=IR-SPEC&Index=1.
(125) NIST. Octafluoro-cyclobutane (C4F8) 2023 https://webbook.nist.gov/cgi/cbook.cgi?ID=C115253&Mask=80.
(126) Alcaraz, A. N.; Codnia, J.; Azcárate, M. L. SiF4 IR Photodissociation: Gas phase reactions of SiF with CH. *J. Photochem. Photobiol., A* **2009**, *205* (2−3), 79−83.
(127) NIST. Pentadecafluorooctanoic acid 2023 https://webbook.nist.gov/cgi/cbook.cgi?ID=C335671&Units=SI&Mask=80.
(128) Pretsch, E.; Bühlmann, P.; Badertscher, M. *Structure Determination of Organic Compounds: Tables of Spectral Data*, 4th ed.; Springer: Berlin, 2009; Vol. *XV*, p 433.

https://doi.org/10.1021/acs.est.4c05782
Environ. Sci. Technol. XXXX, XXX, XXX−XXX

(129) Andrews, L.; Johnson, G. L. Fourier-transform infrared spectra of hydrogen fluoride ((HF)n) species in solid argon. *J. Phys. Chem. A* **1984**, *88* (3), 425−432.
(130) Ooe, H.; Miyamoto, Y.; Kuma, S.; Kawaguchi, K.; Nakajima, K.; Nakano, I.; Sasao, N.; Tang, J.; Taniguchi, T.; Yoshimura, M. Diffusion of hydrogen fluoride in solid parahydrogen. *J. Chem. Phys.* **2013**, *138* (21), No. 214309.
(131) Adi, M. A.; Altarawneh, M. Thermal decomposition of heptafluoropropylene-oxide-dimer acid (GenX). *Chemosphere* **2022**, *289*, No. 133118.
(132) Dolatabad, A. A.; Sun, R.; Cao, J.; Mai, J.; Zhang, X.; Lei, Z.; Litvanova, K.; Kubatova, A.; Xiao, F. Thermal Degradation of Long-chain Fluorinated Greenhouse Gases: Stability, Byproducts, and Remediation Approaches *ACS ES&T Eng.* 2024 DOI: 10.1021/acsestengg.4c00535.
(133) Wang, J. L.; Abusallout, I.; Song, M. R.; Marfil-Vega, R.; Hanigan, D. Quantification of per- and polyfluoroalkyl substances with a modified total organic carbon analyzer and ion chromatography. *AWWA Water Sci.* **2021**, *3* (4), e1235 DOI: 10.1002/aws2.1235.
(134) Jin, Z. Q.; Tian, B.; Wang, L. W.; Wang, R. Z. Comparison on Thermal Conductivity and Permeability of Granular and Consolidated Activated Carbon for Refrigeration. *Chin. J. Chem. Eng.* **2013**, *21* (6), 676−682.
(135) Khaliji Oskouei, M.; Tamainot-Telto, Z. Investigation of the heat transfer properties of granular activated carbon with R723 for adsorption refrigeration and heat pump. *Therm. Sci. Eng. Prog.* **2019**, *12*, 1−12.
(136) Wang, J. L.; Tran, L. L.; Mendoza, J.; Chen, K. P.; Tian, L. H.; Zhao, Y. W.; Liu, J. Y.; Lin, Y. H. Thermal transformations of perfluorooctanoic acid (PFOA): Mechanisms, volatile organofluorine emissions, and implications to thermal regeneration of granular activated carbon. *J. Hazard. Mater.* **2024**, *479*, 135737 DOI: 10.1016/j.jhazmat.2024.135737.
(137) Krug, J. D.; Lemieux, P. M.; Lee, C. W.; Ryan, J. V.; Kariher, P. H.; Shields, E. P.; Wickersham, L. C.; Denison, M. K.; Davis, K. A.; Swensen, D. A.; Burnette, R. P.; Wendt, J. O. L.; Linak, W. P. Combustion of C1 and C2 PFAS: Kinetic modeling and experiments. *J. Air Waste Manage Assoc.* **2022**, *72* (3), 256−270.

https://doi.org/10.1021/acs.est.4c05782
Environ. Sci. Technol. XXXX, XXX, XXX−XXX